High-efficiency machining of single-crystal germanium using large-radius diamond tools

Tsutomu Ohta

Mitsubishi Electric Corporation,
Kamakura Works, 325 Kamimachiya,
Kamakura, Kanagawa 247-8520, Japan

Jiwang Yan*

Department of Nanomechanics,
Tohoku University, Aramaki Aoba 6-6-01,
Aoba-ku, Sendai 980-8579, Japan
E-mail: yanjw@pm.mech.tohoku.ac.jp
*Corresponding author

Shuuma Yajima

Mitsubishi Electric Corporation,
Kamakura Works, 325 Kamimachiya,
Kamakura, Kanagawa 247-8520, Japan

Youichi Takahashi

Tokyo Diamond Tools Mfg. Co., Ltd,
3-5 Nakane 2chome, Meguroku,
Tokyo 152-0031, Japan

Naoyuki Horikawa

Tokyo Diamond Tools Mfg. Co., Ltd,
340-3 Imai, Okaya,
Nagano 394-0001, Japan

Tsunemoto Kuriyagawa

Department of Nanomechanics,
Tohoku University, Aramaki Aoba 6-6-01,
Aoba-ku, Sendai 980-8579, Japan

Abstract: Round-nosed diamond tools with various nose radii are used for cutting single crystalline germanium and fundamental machining characteristics are examined. It is found that when cutting with small radius tools, the principal cutting force is dominant and crater wear on rake face is significant. However, when cutting with large radius tools, the thrust force

becomes significant and tool failure is caused by formation of an angular flank wear land. The use of a large radius tool at a high tool feed improves ductile machining efficiency by a factor of over ten, thus is useful for reducing infrared lens manufacturing costs.

Keywords: germanium; infrared lens; diamond turning; ductile machining; tool wear; cutting force; tool radius.

Reference to this paper should be made as follows: Ohta, T., Yan, J., Yajima, S., Takahashi, Y., Horikawa, N. and Kuriyagawa, T. (2007) 'High-efficiency machining of single-crystal germanium using large-radius diamond tools', *Int. J. Surface Science and Engineering*, Vol. 1, No. 4, pp.374–392.

Biographical notes: Tsutomu Ohta graduated from Ritsumeikan University with a Bachelors Degree in 1986 and a Masters Degree in 1988 both in Mechanical Engineering. He joined Mitsubishi Electric Corp. Kamakura Works, in 1988. He has been a Manager since 2001 and a Manager of Machining and Fabrication Section since 2007. He is a Doctor course student in Tohoku University since 2006. He has been engaged in development of high-efficiency precision machining.

Jiwang Yan is an Associate Professor in the Department of Nanomechanics, Graduate School of Engineering, Tohoku University. His research interests include ultraprecision machining of optical and optoelectronic materials, design and fabrication of nanostructural surfaces, micro/nanomachining mechanics, laser processing of crystals and semiconductors, and tooling technology using diamond and diamond-related materials in manufacturing applications.

Shuuma Yajima graduated from Waseda University with a Master's Degree in 2002 and a Bachelor's Degree in 2000, both in Mechanical Engineering. He joined Mitsubishi Electric Corp. Kamakura Works, in 2002. He has been engaged in development of precision machining.

Youichi Takahashi graduated from Miyagi National College of Technology, Mechanical Engineering in 1978. He joined Sendai factory, Tokyo diamond tools Mfg. Co., Ltd. Miyagi, Japan. He has been engaged in the design, production of single-crystalline and sintered diamond tools. He has been a Manager of Sales Engineering Group for Diamond Tools since 2001.

Naoyuki Horikawa graduated from Okaya technical high school, Mechanical Engineering in 1971. He joined Tokyo diamond tools Mfg. Co., Ltd. Japan. He has been engaged in the manufacturing engineering of diamond tools, especially tool polishing. He has been a manager of diamond stone centre since 2005.

Tsunemoto Kuriyagawa is a Professor in the Department of Nanomechanics, Graduate School of Engineering, Tohoku University, Japan. His research interests include nanoprecision mechanical fabrication and Micro/Meso Mechanical Manufacturing (M4 process).

1 Introduction

Recently, infrared optical lenses are required more and more in various industrial fields such as night vision systems of vehicles and dark field sensing systems for security. Infrared optical lenses are usually made of brittle materials such as single-crystalline germanium and silicon (Suzuki et al., 1997; Yan et al., 2002a, 2005). Although new infrared transparent materials other than silicon and germanium are being developed and press-moulding technology has been attempted to be used to fabricate infrared lenses at a relatively low production cost, those new materials are still expensive. Generally, the newly developed materials must be moulded at a high temperature; thus, the life of the moulding die is very limited, and in turn, the expense of the pressing moulds is very high. For these reasons, the press-moulding technology has not yet been widely spread into the infrared optical manufacturing industry. Currently, the fabrication of infrared lenses is still dependent on material removal processes.

Conventional infrared lenses are of spherical shape and are manufactured by grinding and polishing. Recently, aspherical lenses and Fresnel lenses are required more and more, and these complicated shaped lenses are mainly manufactured by diamond turning (Yan et al., 2002a, 2005). In the diamond turning of germanium, a crack-free surface can be obtained by controlling the machining mode in a ductile one (Nakasuji et al., 1990; Blake and Scattergood, 1990; Yan et al., 2004, 2006). For most of diamond turning processes, grinding is usually used as a premachining step. In a previous paper, in order to minimise the depth of material removal for diamond turning, the present authors proposed a method to predict the subsurface damage depth by surface profiling based on the inherent relationship between the surface roughness and the subsurface damage depth (Ohta et al., 2007).

Conventionally, in the ductile machining of silicon and germanium lenses, a small radius round-nosed diamond tool with high form accuracy has been used under 2-axis numerical control, as shown in Figure 1(a) where a detailed presentation of Section A is shown in Figure 1(b). The tool radius is usually about 1 mm or much smaller (Nakasuji et al., 1990; Blake and Scattergood, 1990). To obtain a crack-free surface using this kind of tools, tool feed f must be extremely small (1–3 μm/rev). Also, the workpiece spindle rotation rate is usually set to the range from 1000 rpm to 2000 rpm, lower than the maximum rotation rates of the machine tools. This is probably because a high spindle rotation rate leads to a high cutting speed, which causes severe tool wear. As a result, ductile machining by this method is inefficient with a very low material removal rate.

To conduct ductile machining efficiently, diamond turning of brittle materials using a straight-nosed diamond tool has been proposed, which has been successfully used in the fabrication of convex aspherical lenses on single-crystalline silicon and germanium on 3-axis numerically controlled machine tools (Yan et al., 2002a). In this method, undeformed chip thickness is determined by the tool feed and cutting edge angle. Therefore, ductile material removal at large tool feeds can be achieved by using a sufficiently small cutting edge angle (Yan et al., 2002b).

However, for the straight-nosed tools, it is difficult to generate concave surfaces because of the interference between the tool and the workpiece. In this work, we attempt to conduct high-efficiency ductile machining of germanium with a large-radius round-nosed diamond tool to solve the problems mentioned above. The tool nose radius used in the present experiments ranges from a few millimetres to a few tens of millimetres, far larger than that of the conventional tools (~1 mm). We used a tool feed

rate about five times higher than the conventional one and a spindle rotation rate about three times the conventional one (~5000 rpm). Theoretically, these conditions give rise to a material removal rate 15 times higher than that of the conventional process. It is expected that this method can achieve both high production efficiency and high surface quality. The objective of this paper is to experimentally investigate fundamental characteristics of the machining process such as cutting forces and tool wear, and make comparisons with conventional methods and with silicon machining.

Figure 1 Cutting models for a round-nosed diamond tool: (a) 2-axis control diamond turning model and (b) material removal model

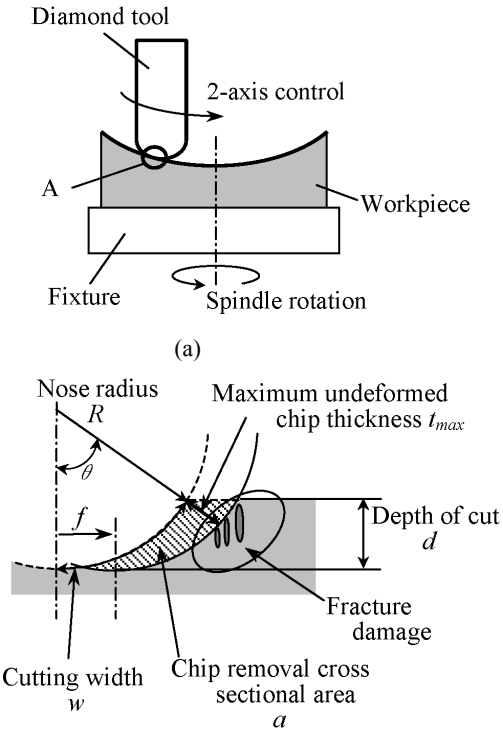

2 Experimental procedure

Experiments were carried out on a Precitech Nanoform-200 ultraprecision diamond turning machine. This machine has a hydrostatic bearing spindle and two perpendicular hydrostatic slide tables along the *X*-axis and *Z*-axis. Those table-driving systems are linear AC synchronous motors. A diamond cutting tool was set onto the rotary *B*-axis. The operation principle of the diamond turning is schematically shown in Figure 2. To measure the micro-cutting forces, a three-component piezoelectric sensor (Kistler 9257B) was used as a dynamometer, which was equipped under the tool holder, as shown in Figure 3.

Figure 2 Schematic of diamond turning operation

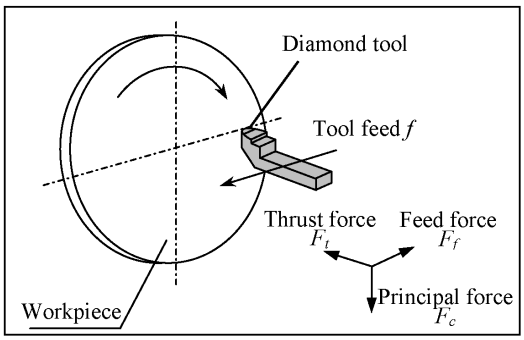

Figure 3 Photograph of the ultraprecision diamond turning machine equipped with a piezoelectric dynamometer

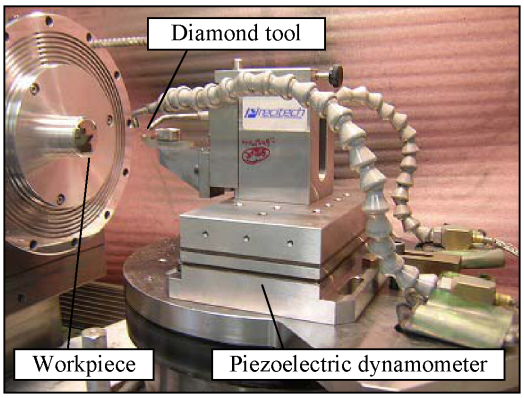

Single-crystal germanium (111) lens substrates were used as specimens. These workpieces are 78 mm in diameter and 8 mm in thickness. Diamond tools used in the experiments are made of single-crystal natural diamond and have different nose radius, from 1.15 mm to 86.43 mm, as listed in Table 1. Figure 4 is a Scanning Electron Microscope (SEM) photograph of the tool with a nose radius of 66.03 mm. All these tools have –25° rake angles and 10° relief angles. The cutting plane of the tools are oriented to the (110) planes of diamond crystals. The flank faces of the tools were approximately along the (100) planes. The machining conditions used for each tool are also listed in Table 1. In the experiments, the tool no. 1 was used to estimate tool life under the conventional cutting conditions. Other tools were used for high-efficiency cutting conditions. In the table, calculated values of cutting width w, maximum undeformed chip thickness t_{max}, and chip cross-sectional area a are also listed. Calculations are based on the following equations and the definition of the symbols can be found in Figure 1(b).

$$w = R\theta \tag{1}$$

$$t_{\max} = \frac{f}{R}\sqrt{2Rd - d^2} \tag{2}$$

$$a = wt_{\max}/2. \tag{3}$$

Table 1 Machining conditions used for various tools

Tool no.	*Tool radius* (mm)	*Cutting conditions*			*Cutting width* (μm)	*Maximum undeformed chip thickness* (nm)	*Chip cross-sectional area* (μm^2)
		Depth of cut (μm)	*Feed rate* (mm/min)	*Spindle rotation rate* (rpm)			
1	1.15	3	1.8	1600	83	72	3.0
2	10.91				256	117	15.0
3	11.22				260	116	15.0
4	11.61	3	25	5000	263	114	15.0
5	66.03				629	48	15.0
6	86.43				720	42	15.0

Figure 4 SEM photograph of a diamond tool with a nose radius of 66.03 mm

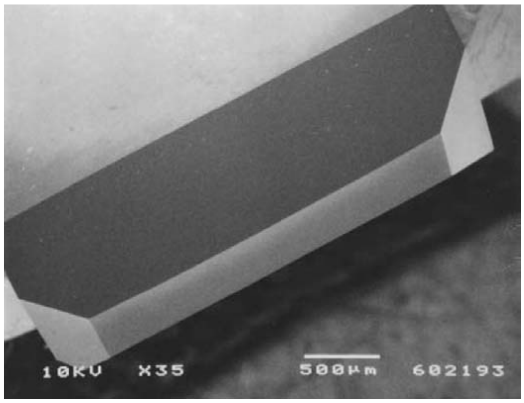

Before and after machining, the diamond tools were observed using an SEM JEOL-T330A. Cross-sectional profiles of the main cutting edges were measured by an electron beam three-dimensional surface roughness analyser Elionix ESA-3000 (Asai et al., 1990). This analyser has a pair of secondary electron detectors, and can create an image of a sectional curve for a diamond tool edge. By this means, the changes in the tool geometry caused by tool wear can be precisely evaluated. In this paper, the tool life is defined as the effective cutting distance before micro-cracks are generated on the workpiece surface.

Figure 5 schematically shows the normal wear geometry of a diamond tool when machining germanium. The tool wear can be roughly divided into three kinds: crater wear in tool rake face, edge roundness, and flank wear. The flank wear can be further divided into two parts: primary flank wear and secondary flank wear. The primary flank wear land is parallel to the cutting direction; whereas the secondary flank wear is the curved part caused by the friction between the tool and the workpiece surface behind the tool due to elastic recovery of the workpiece material. The secondary flank wear will be significant especially when a highly negative rake angle is used, because a highly negative rake angle causes workpiece materials to flow downwards the cutting tool and to recover after the tool has passed. Sometimes, the boundary between two flank wear sections is difficult to distinguish, especially at the beginning of cutting; thus, in this case, the total wear width of flank face was measured to evaluate the tool wear performance.

Figure 5 Schematic presentation of typical cross-section geometry of a cutting edge after tool wear

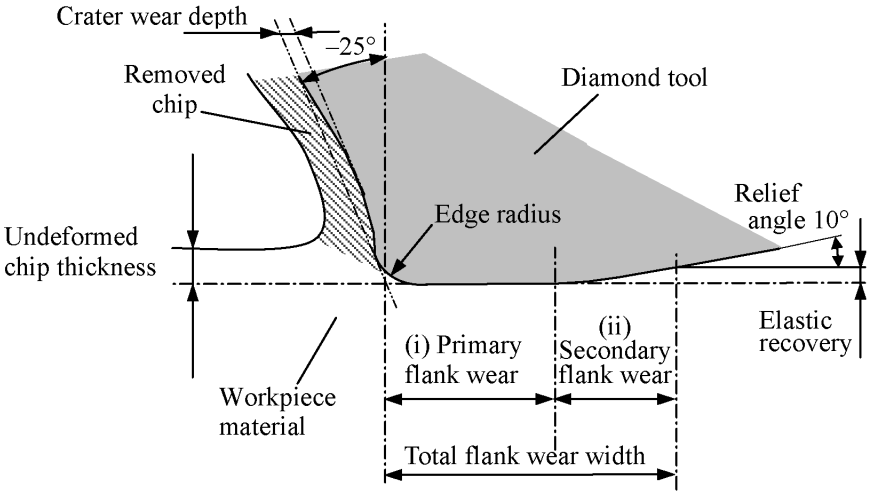

3 Results and discussion

3.1 Results of conventional cutting

First, cutting experiments were done under the conventional cutting conditions using a 1.15 mm nose radius diamond tool (tool no. 1). It was found that micro-cracks began to occur slightly on the machined surface at a cutting distance of 1020 km. This cutting distance is then decided as the tool life. It is noticed that this distance is far longer than that of silicon machining (Yan et al., 2003; Li et al., 2005; Durazo-Cardenas et al., 2007), which indicates that in germanium machining diamond tool wear is insignificant compared with silicon machining.

The change of cutting forces with cutting distance is shown in Figure 6. It is seen that the principal cutting force F_c is dominant in the process, whose value reaches 0.36 N at the cutting distance near the tool life. The thrust force F_t and the feeding force F_f was 0.2 N and 0.03 N, respectively, remarkably smaller than the principal force. Also, it is noted that the feed force almost kept constant during the cutting process. In silicon cutting, the thrust cutting force was dominant rather than the principal cutting force (Yan et al., 2003; Durazo-Cardenas et al., 2007). This significant difference might be due to the difference in workpiece materials property and tool geometry changes after tool wear.

SEM photographs of the main cutting edges of the diamond tool before cutting and after cutting for 1020 km are shown in Figure 7(a) and (b), respectively. Before cutting, an extremely sharp cutting edge can be seen between the rake face and the flank face, as shown in Figure 7(a). After machining, extremely small chippings in the submicron level occurred to the cutting edge. A 0.5 μm wide slight crater wear is observed on the rake face. It is also noticeable that the rake face area adjacent to the crater wear has been roughened. In the photograph, no apparent flank wear is shown, which is distinctly different from the phenomena in silicon machining (Yan et al., 2003; Li et al., 2005).

Figure 6 Changes of cutting forces under conventional cutting conditions

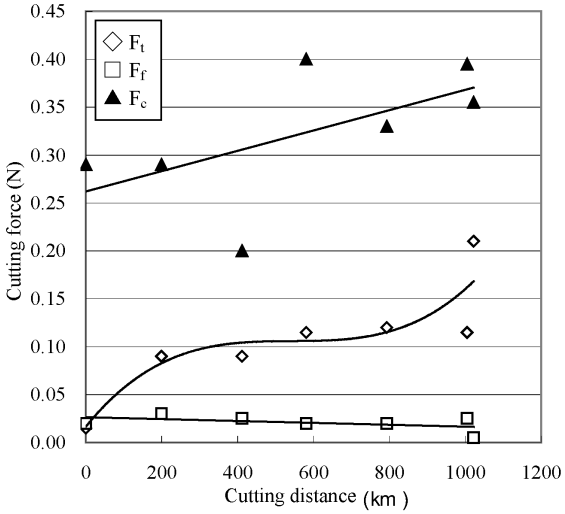

Figure 7 SEM photographs of the main cutting edge of a diamond tool with a 1.15 mm nose radius: (a) new tool and (b) after cutting for 1020 km

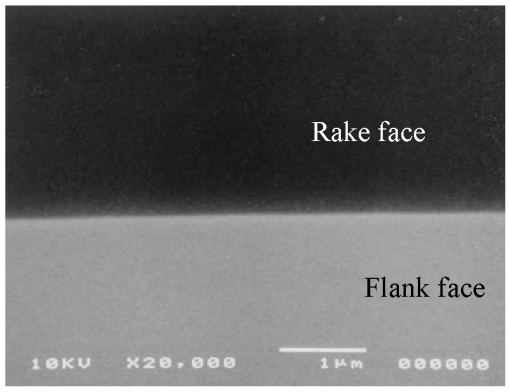

(a)

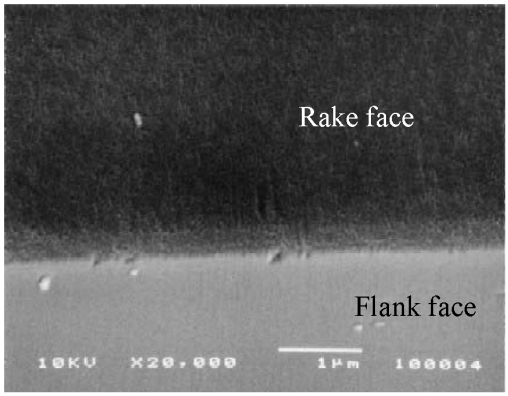

(b)

The cross-sectional profile of the same cutting edge was measured as shown in Figure 8. The depth and the width of crater wear on the rake face are 0.06 μm and 0.5 μm, respectively. The flank wear, which is parallel to the cutting direction, is about 0.17 μm, considerably smaller than the crater wear. The tool edge radius is approximately 0.1 μm. This wear geometry is distinctly different from that in silicon machining. It was reported that flank wear in silicon cutting was very significant (2 μm at 5 km cutting distance (Yan et al., 2003), and 6 μm at 30 km cutting distance (Durazo-Cardenas et al., 2007)).

Figure 8 Cross-sectional profile of main cutting edge of the 1.15 mm nose radius tool at a cutting distance of 1020 km

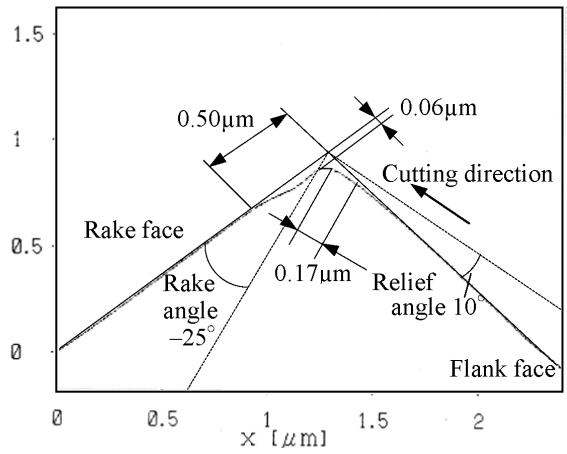

It is noteworthy that the width of the crater wear (0.5 μm) is seven times the maximum undeformed chip thickness (0.072 μm). Therefore, it is conceivable that chips have been rubbing on the rake face severely, causing the deep crater wear. The roughened area adjacent to the crater wear might be the early stage of crater wear. From this aspect, we can assume that the increase of cutting force during germanium machining is caused by the severe friction between the chips and the rake face. Crack generation on the workpiece surface in this case may be due to the combined effects of two aspects: one is the difficulties in chip flow along the rake face, and the other is the increase of tensile stress behind the tool caused by the friction force occurring at the flank wear land.

3.2 Results of high-efficiency cutting

3.2.1 Surface texture and cutting force

Next, cutting experiments were done using a large-radius diamond tool (tool no. 3) with a nose radius of 11.22 mm. It was found that after cutting for a distance of about 160 km, abnormal features began to occur on the machined surface. The abnormal features involve scaled waviness and micro-fractures or cracks. Figure 9 shows a Nomarski micrograph of a crack-free surface at the beginning of cutting using the new tool. Figure 10(a) and (b) show micrographs of the surfaces with scaled waviness and micro-cracks, respectively, after cutting for a distance of 160 km. The scaled waviness was found to occur before the occurrence of micro-cracks.

Figure 9 Nomarski micrograph of crack-free surface of germanium

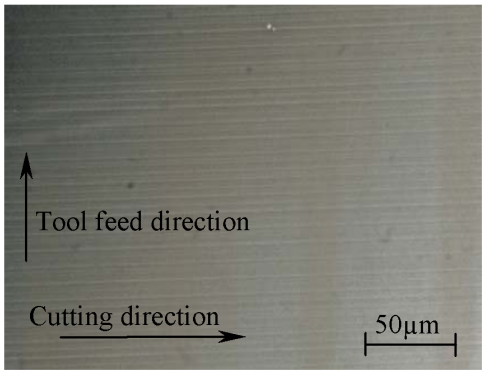

Figure 10 Micrographs of surface textures after machining for 160 km with a large nose radius tool: (a) scaled waviness surface and (b) cracked surface

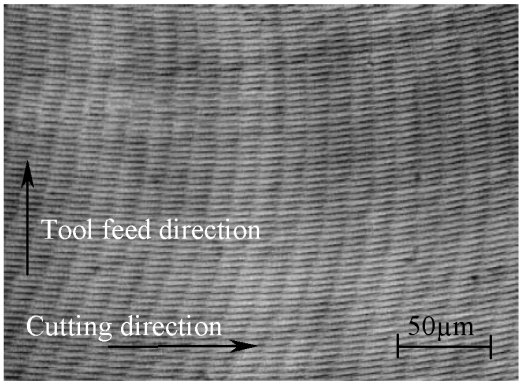

(a)

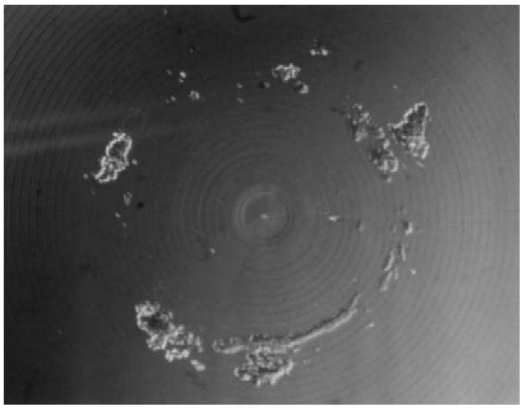

(b)

Typical cutting force signals at a cutting distance of 160 km are shown in Figure 11 where the horizontal axis is time and the vertical axis is the force. The measurements lasted for about 90 s during one cutting pass through the whole workpiece.

Slight increases in forces can be seen and fluctuations occurred indicating the unsteadiness of the cutting process after tool wear.

Figure 11 Cutting force signals at a cutting distance of 160 km

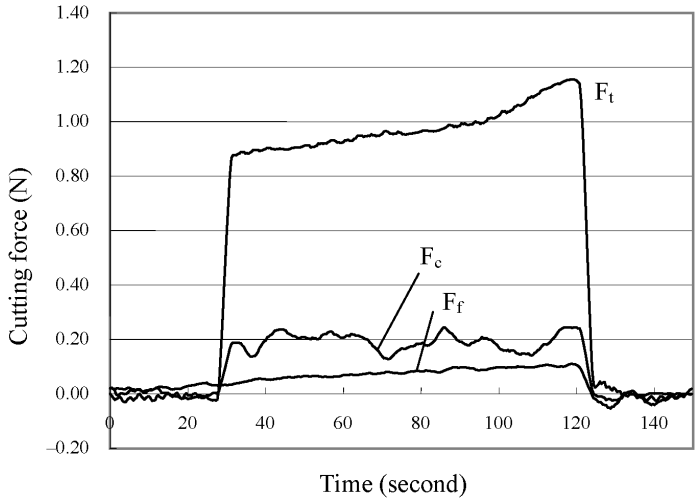

The changes of forces with cutting distance until 160 km are shown in Figure 12. It can be seen that the thrust force increases rapidly after cutting for about 40 km, while the principal cutting force and the feed force keep almost constant. The thrust force at 160 km was about 0.9 N, 2.3 times that of the conventional cutting at 1020 km (0.4 N). The trends of force changes are very different from that of the conventional cutting with small radius tools, which indicates possible differences in machining mechanism and tool wear mechanisms. These issues will be discussed later in this paper.

Figure 12 Changes of cutting forces with cutting distance when machining with a large-radius tool

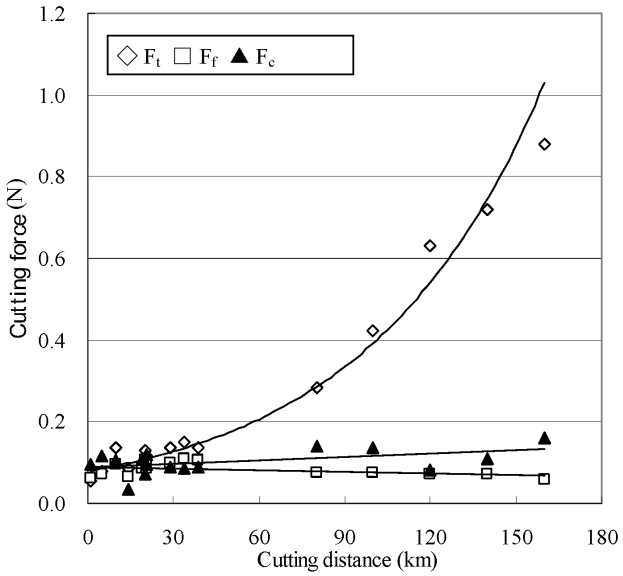

3.2.2 Effects of tool nose radius

To investigate the effects of tool nose radius on machining performance, experiments were done with tools of different nose radii. Tools no. 3–6, whose nose radius changes from 11.22 mm to 86.43 mm, were used. To reduce experiment numbers, cutting tests were done until a cutting distance of 38.4 km, which is within the region of stable cutting, as can be seen from Figure 12. The effects of tool nose radius on principal cutting force, thrust force, and feed force are shown in Figures 13–15, respectively.

Figure 13 Effects of tool nose radius on principal forces F_c

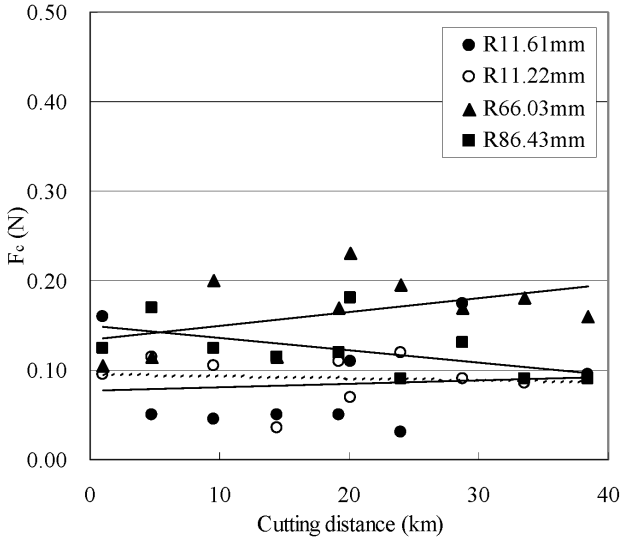

Figure 14 Effects of tool nose radius on thrust forces F_t

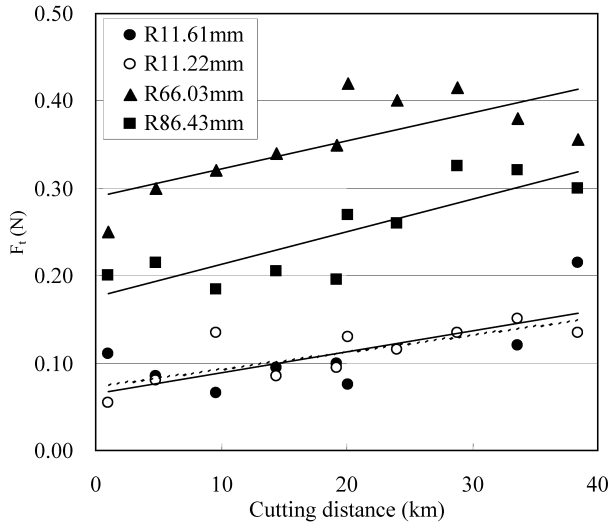

Figure 15 Effects of tool nose radius on feed forces F_f

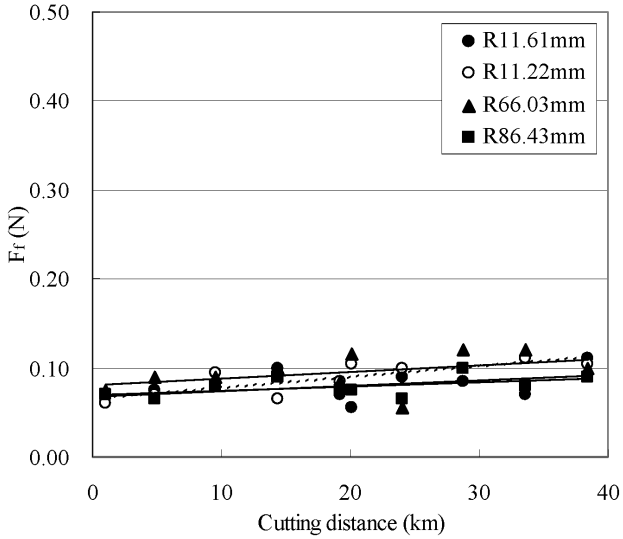

As shown in Figure 13, principal forces of 66.03 mm and 86.43 mm tools tend to be larger than the 11.22 mm and 11.61 tools. The same trend can be seen more clearly in the results of thrust forces as shown in Figure 14, despite that there is a reverse order between the 66.03 mm and 86.43 mm tools, which might be caused by differences in initial tool conditions such as edge sharpness and so on. A general tendency is that the larger the tool nose radius is, the bigger the cutting force is. This effect may be due to the fact that if other conditions are the same, a larger nose radius causes a bigger cutting width, namely, contact length between tool and workpiece. However, as shown in Figure 15, feed forces of all tools are almost in the same level and do not show obvious change with cutting distance. As known in conventional metal cutting, feed force is remarkably lower than principal force and thrust force, which is dependent on tool feed rate and independent of tool nose radius.

3.2.3 Tool wear characteristics

The cutting edge of tool no. 3 (nose radius 11.22 mm) was observed. Figure 16(a) and (b) show the SEM photographs of the edge at cutting distances of 38.4 km and 160 km, respectively. In Figure 16(a), there is a slight flat wear land at the flank face while the rake face remains smooth. The flank wear land grows with increase in cutting distance and becomes very wide at 160 km cutting distance. The wear land width of 160 km is about 0.5 μm, which is about three times that of small nose radius tool at 1020 km under conventional cutting conditions as shown in Figure 7(b). The rake face in Figure 16(b) has a similarly roughened texture to that in Figure 7(b), indicating severe friction between tool and chip. What should point out is that in the middle of photograph of Figure 16(b), there is a sudden change in wear land width. This change occurred due to the resetting error of the tool after SEM observation and profile measurement at a distance of 44 km. It is noteworthy that in both photographs, there is no visible micro-chippings on the cutting edge, and the flank wear lands are smooth without micro-grooves like that seen in cutting silicon (Yan et al., 2003; Li et al., 2005).

Figure 16 SEM photographs of cutting edge of a large nose radius tool at different cutting distances: (a) 38.4 km and (b) 160 km

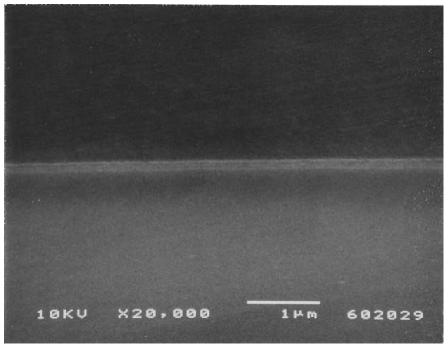

(a)

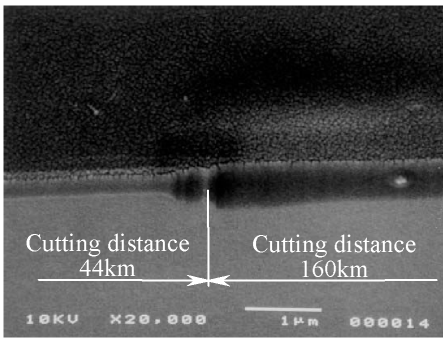

(b)

Figure 17 shows a cross-sectional profile of the cutting edge of tool no. 2 with a nose radius of 10.91 mm after cutting for a distance of 8.5 km. Figure 18 shows the profile of tool no. 4 (nose radius 11.61 mm) at 38.4 km. It can be seen that the cross-sectional profiles in both the figures are very similar. In either case, the cutting edge has retreated for about 0.1 μm from the initial state. The total flank wear width was approximately 1.0 μm, where the boundary of primary and secondary flank wear were not obviously observed. These results indicate that the early stage wear of the large-radius diamond tools is flank wear, different from that of the small radius tool.

Figure 19 shows the cutting edge cross-sectional profile of tool no. 3 (nose radius 11.22 mm) after a cutting distance of 160 km. This figure corresponds to the right side of the SEM photograph in Figure 16(b). In the profile, a shallow crater wear has extended to about 1 μm far from the cutting edge. It is noted that the retreat of cutting edge is apparently larger than those in Figures 17 and 18. At the same time, the flank wear is significant where the boundary between the primary and the secondary flank wear can be clearly seen. The primary flank wear width is approximately 0.3 μm, and the secondary flank wear width is 0.5 μm. The total flank wear width is almost the same as those in Figures 17 and 18, indicating that the width of flank wear did not grow further with cutting distance. However, unlike conventional primary flank wear lands, which are parallel to the cutting direction, in the present case, there is a small angle (approximately 10°) between the wear land and the cutting direction. In this paper,

we term this kind of wear the angular flank wear. This wear geometry causes a highly negative effective rake angle to approximately –80°.

Figure 17 Cross-sectional profile of cutting edge of the tool with a radius of 10.91 mm at a cutting distance of 8.5 km

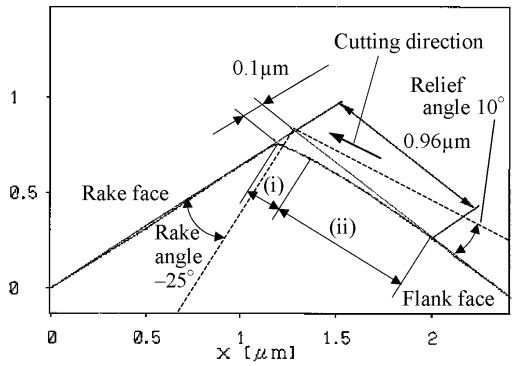

Figure 18 Cross-sectional profile of cutting edge of the tool with a radius of 11.61 mm at a cutting distance of 38.4 km

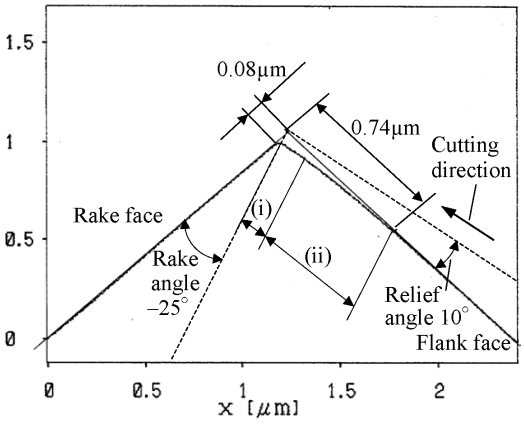

Figure 19 Cross-sectional profile of cutting edge of the tool with a radius of 11.22 mm at a cutting distance of 160 km

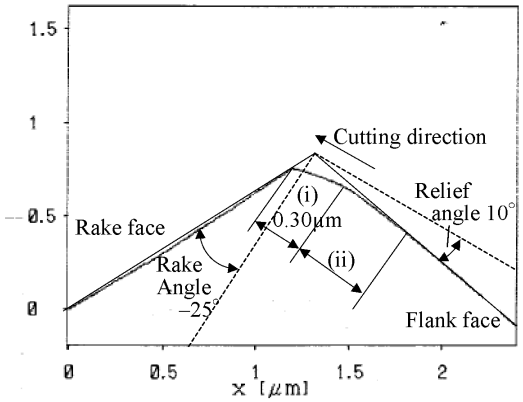

This situation can be schematically shown in Figure 20. As the effective rake angle becomes highly negative, chip flow in front of the tool will be obstructed and the unfavourable downward flow will occur, which is similar to metal cutting and silicon cutting (Komanduri, 1971; Yan et al., 2000). The downward flow of material will lead to a large elastic/plastic deformation layer beneath the tool. This deformation layer cannot cause brittle fracture if the undeformed chip thickness is extremely small, but can cause periodical features like scaled waviness shown in Figure 10(a) on the machined surface due to the stick–slip phenomenon. However, when the undeformed chip thickness is sufficiently large, after the tool passes the residual tensile stress will cause lateral crack initiation along the plastic–elastic boundary (Yan et al., 2000), leading to micro-fractures as shown in Figure 10(b). This type of fracture corresponds to a large cutting force owing to the formation of a thick plastically deformed layer (subsurface damage layer) and increased surface roughness.

Figure 20 Schematic of cutting edge cross-sectional profile with an angular flank wear land

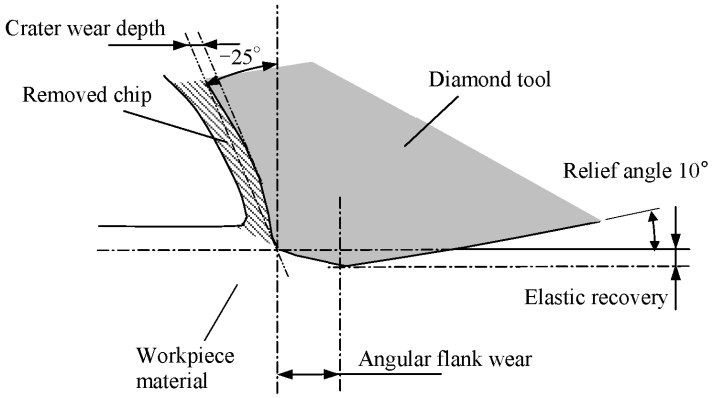

It has been known that in silicon machining, after cutting for a few kilometres, micro-grooves begin to be generated on the flank wear land, which accelerates the retreat of cutting edge and finally causes total failure of the tool (Yan et al., 2003; Li et al., 2005; Durazo-Cardenas et al., 2007). In this work, we demonstrated that in germanium machining, the flank wear lands remain smooth without apparent chippings and micro-grooves even after cutting for over 100 km. The factor causing tool failure is the formation of an angular flank wear land, which generates an excessively high negative rake angle. This fact indicates distinct differences in the tool–workpiece material interaction during cutting silicon and germanium with diamond tools. It is assumed that the chemical and electrical effects that have been significant in silicon machining are less significant in germanium machining. This feature has verified that diamond turning provides a high-efficiency production method for ultraprecision germanium optical components.

The differences in tool wear geometry between small-radius tools and large-radius tools are thought to be caused by thermal effects. A large-radius tool corresponds to a large cutting width (tool–chip contact length) and a large chip cross-sectional area if other conditions are the same. This tool–workpiece contact situation will cause more heat generation than the small-radius tools. Additionally, higher spindle rotation rates are used for large-radius tools, which is also a reason for temperature rise. High-temperature

material flow causes the sharp edge to be rounded and to retreat rapidly, leading to the formation of angular flank wear land.

Table 2 shows a comparison of productivity between the conventional cutting with small-radius tools and high-efficiency cutting with large nose radius tools. A small-radius tool has a significantly longer tool life than a large-radius tool in terms of cutting distance. On the other hand, owing to that small tool feed rates must be used when cutting with a small-radius tool, the necessary cutting distance and cutting time taken to finish one workpiece is remarkably longer than that of larger-radius tools. As a result, there is no distinct difference in the number of workpieces which can be machined with one tool. However, the point to note is that the time needed for finishing one workpiece with the large-radius tool is about 1/14 of that of the small-radius tool. In other words, the production efficiency of the proposed method using large-radius tools is significantly higher than the conventional method. Therefore, it is possible to reduce the total manufacturing cost of infrared germanium lenses using the high-efficiency cutting conditions presented in this paper.

Table 2 Comparison of productivity between conventional cutting with small radius tools and high-efficiency cutting with large-radius tools

Tool type	*Tool life* (km)	*Cutting distance for a ϕ78 mm workpiece* (km)	*Number of workpiece cut with one tool* (*pieces*)	*Cutting time for a ϕ78 mm workpiece* (min)
Small nose radius (~1 mm)	1020	4.78	209	21.7
Large nose radius (~80 mm)	160	0.96	166	1.56

4 Conclusions

Round-nosed diamond tools of various nose radii were used for cutting single-crystalline germanium at an undeformed chip thickness ranging from a few tens of nanometres to the submicron level. Fundamental characteristics of the machining process such as cutting forces and tool wear were examined experimentally. The conclusions are summarised as follows.

- In the cutting with small-radius tools (~1 mm) under small-feed conditions, tool wear is very slow and steady where crater wear on rake face becomes dominant; while flank wear is small. Cater wear growth and rake face roughening cause difficulties in chip flow and increase of cutting forces.
- In the cutting with large-radius tools (~80 mm) at high-feed and high-speed conditions, the tool life in terms of cutting distance is shorter than that of small-radius tools. The tool failure is caused by formation of an angular flank wear land, which generates an excessively high negative effective rake angle.
- In the cutting with small-radius tools, principal cutting force is dominant, while in the cutting with large-radius tools, the thrust force is significant.

- The use of large-radius tools at high tool feed rates provides higher production efficiency by a factor of over 10, despite the decrease in tool life. The proposed machining conditions are useful for reducing infrared lens manufacturing costs.
- Unlike silicon cutting, there is no occurrence of micro-chippings and micro-grooves to the cutting edges in the cutting of germanium, indicating insignificance of chemical or electrical effects in tool wear. The practical tool life for germanium machining is by far longer than that of silicon cutting.

Acknowledgement

This work has been partially supported by the industrial technology research grant program (04A31508) from the Japan New Energy and Industrial Technology Development Organisation (NEDO).

References

Asai, S., Taguchi, T., Horio, K., Kasai, T. and Kobayashi, A. (1990) 'Measuring and analysis on cutting edge radius of single point diamond tools using newly developed scanning electron microscope (SEM)', *Journal of the Japan Society for Precision Engineering*, Vol. 46, No. 7, pp.145–150.

Blake, P.N. and Scattergood, R.O. (1990) 'Ductile regime machining of germanium and silicon', *J. Amer. Ceram. Soc.*, Vol. 73, No. 4, pp.949–957.

Durazo-Cardenas, P., Shore, X., Luo, T., Jacklin, S., Impey, A. and Cox, A. (2007) '3D characterization of tool wear whilst diamond turning silicon', *Wear*, Vol. 262, pp.340–349.

Komanduri, R. (1971) 'Some aspects of machining with negative rake tools simulating grinding', *Int. J. Machine Tool Design and Research*, Vol. 11, p.223.

Li, X.P., He, T. and Rahman, M. (2005) 'Tool wear characteristics and their effects on nanoscale ductile mode cutting of silicon wafer', *Wear*, Vol. 259, pp.1207–1214.

Nakasuji, T., Kodera, S., Hara, S., Matsunaga, H., Ikawa, N. and Shimada, S. (1990) 'Diamond turning of brittle materials for optical components', *Ann. CIRP*, Vol. 39, No. 1, pp.89–92.

Ohta, T., Yan, J., Kuriyagawa, T., Kodera, S. and Nakasuji, T. (2007) 'Prediction of subsurface damage depth of ground brittle materials by surface profiling', *Int. J. Machining and Machining of Materials*, Vol. 2, No. 1, pp.108–124.

Suzuki, H., Kodera, S., Nakasuji, T., Ohta, T. and Syoji, K. (1997) 'Study on aspherical surface polishing of single crystal silicon lens', *Journal of the Japan Society for Precision Engineering*, Vol. 63, No. 9, p.1280.

Yan, J., Syoji, K. and Kuriyagawa, T. (2000) 'Ducticle-brittle transition at large negative tool rake angles', *Journal of the Japan Society for Precision Engineering*, Vol. 66, No. 7, pp.1130–1134.

Yan, J., Syoji, K. and Kuriyagawa, T. (2002a) 'Fabrication of large-diameter single-crystal silicon aspheric lens by straight-line enveloping diamond-turning method', *Journal of the Japan Society for Precision Engineering*, Vol. 68, No. 4, pp.1561–1565.

Yan, J., Syoji, K., Kuriyagawa, T. and Suzuki, H. (2002b) 'Ductile regime turning at large tool feed', *Journal of Materials Processing Technology*, Vol. 121, pp.363–372.

Yan, J., Syoji, K. and Tamaki, J. (2003) 'Some observations on the wear of diamond tools in ultra-precision cutting of single-crystal silicon', *Wear*, Vol. 255, Nos. 7–12, pp.1380–1387.

Yan, J., Maekawa, K., Tamaki, J. and Kubo, A. (2004) 'Experimental study on the ultraprecision ductile machinability of single-crystal Germanium', *JSME International Journal, Series C*, Vol. 47, No. 1, pp.29–36.

Yan, J., Maekawa, K., Tamaki, J. and Kuriyagawa, T. (2005) 'Micro grooving on single-crystal germanium for infrared fresnel lenses', *Journal of Micromechanics and Microengineering*, Vol. 15, pp.1925–1931.

Yan, J., Takahashi, Y., Tamaki, J., Kubo, A., Kuriyagawa, T. and Sato, Y. (2006) 'Ultraprecision machining characteristics of poly-crystalline germanium', *JSME International Journal, Series C*, Vol. 49, No. 1, pp.63–69.